Catalysis Today 164 (2011) 347–352

Contents lists available at ScienceDirect

Catalysis Today

journal homepage: www.elsevier.com/locate/cattod

Single-crystalline mesoporous CaO supported Cr–V binary oxides: Highly active catalysts for the oxidative dehydrogenation of isobutane

Jiguang Deng, Lei Zhang, Caixin Liu, Yunsheng Xia, Hongxing Dai*

Laboratory of Catalysis Chemistry and Nanoscience, Department of Chemistry and Chemical Engineering, College of Environmental and Energy and Engineering, Beijing University of Technology, Beijing 100124, PR China

ARTICLE INFO

Article history:
Available online 3 November 2010

Keywords:
Oxidative dehydrogenation
Single-crystalline mesoporous CaO
Chromium–vanadium binary oxide
Supported multi-component catalyst
Reducibility

ABSTRACT

The three-dimensional mesoporous calcium oxide (*meso*-CaO) supported chromium–vanadium binary oxide catalysts *y*CrO_x/10 wt.% VO_x/*meso*-CaO (i.e., *y*Cr/10V/*meso*-CaO, *y* = 0–4 wt.%; the VO_x and CrO_x weight percentages referred to the mass contents of V_2O_5 and Cr_2O_3 in the catalysts, respectively) were prepared via an incipient wetness impregnation route and characterized by means of XRD, BET, SEM, TEM/SAED (selected-area electron diffraction), Raman, and H_2-TPR (temperature-programmed reduction) techniques. The catalytic performance of the materials was evaluated for the oxidative dehydrogenation (ODH) of isobutane. It is found that the *meso*-CaO and *y*Cr/10V/*meso*-CaO displayed wormhole-like mesoporous structures, VO_x and/or CrO_x were highly dispersed in the form of mono- and polyvanadate or polychromate on the surface of the *meso*-CaO support. The H_2-TPR results indicate that 2Cr/10V/*meso*-CaO exhibited the best low-temperature reducibility among the as-prepared catalysts. Under the conditions of isobutane/oxygen molar ratio = 1/2, space velocity = 30,000 mL/(g h), and temperature = 540 °C, a maximal C_4-olefins yield of 15% with the corresponding C_4-olefins selectivity of 79% was achieved over the 2Cr/10V/*meso*-CaO catalyst. It is concluded that the good dispersion of CrO_x and VO_x domains and low-temperature reducibility of the catalyst as well as the strong basicity and three-dimensional wormhole-like mesoporosity of the CaO support were responsible for the excellent catalytic performance of 2Cr/10V/*meso*-CaO for the ODH of isobutane.

1. Introduction

It has been generally accepted that catalytic performance of a supported transition-metal oxide for the oxidative dehydrogenation (ODH) of alkanes is dependent upon the nature of active phase and support [1]. Among the transition-metal oxides, CrO_x, VO_x, and MoO_x are more appropriate as active phase [1–4]. Alkaline materials, such as MgO, Al_2O_3, and ZrO_2, are good candidates for the use as support [3,5–8]. Most of basic supports investigated so far, however, possess low surface areas due to the absence of porous structures. Such bulk materials are unfavorable for the dispersion of active components. Therefore, it is highly desirable to develop a novel strategy for the fabrication of mesoporous alkaline supporting materials with high surface areas. CaO is an important material with strong basicity. To the best of our knowledge, there have been no reports in the literature on the use of single-crystalline mesoporous CaO supported CrO_x–VO_x catalysts for the ODH of alkanes.

Previously, we observed that single transition-metal oxides (e.g., CrO_x) [9,10] and binary transition-metal oxides (e.g., CrO_x–MoO_x) [11] could be highly dispersed on the surfaces of nanosized $Ce_{0.60}Zr_{0.35}Y_{0.05}O_2$ solid solution and ordered mesoporous silica (SBA-15 and MgO-coated SBA-16). These materials showed good activities for the ODH of isobutane. As an extension of our work, we have recently adopted the surfactant-assisted hydrothermal strategy to successfully generate numerous single-crystalline CaO and MgO materials that possessed wormhole-like mesoporous structures and high surface areas [12,13]. In this work, we report the making, characterization, and excellent catalytic performance of single-crystalline wormhole-like mesoporous CaO supported CrO_x–VO_x catalysts for the ODH of isobutane.

2. Experimental

2.1. Catalyst preparation

The single-crystalline wormhole-like mesoporous CaO support was fabricated using the surfactant-assisted hydrothermal dissolution-recrystallization strategy with bulk CaO powders as calcium source. The typical fabrication procedure is as follows: 3.45 g of polyethylene glycol (PEG, $M_{aver.}$ = 1000, Sinopharm Chemical Reagent Co., 99.5%) was first dissolved in 80 mL of deionized water, then 1.12 g of CaO powders (Beijing Chemical Plant, 99%)

* Corresponding author: Tel.: +86 10 6739 6588.
E-mail address: hxdai@bjut.edu.cn (H. Dai).

0920-5861/$ – see front matter © 2010 Elsevier B.V. All rights reserved.
doi:10.1016/j.cattod.2010.10.023

was added to the solution. The molar ratio of CaO to surfactant (PEG) was 1/1.25. After ultrasonic stirring for 24 h, the mixed solution was transferred to a 100-mL Teflon-lined stainless steel autoclave (packed volume = 80 mL), and the autoclave was placed in an oven for hydrothermal treatment at 240° C (the estimated pressure, 15–20 atm) for 72 h. The obtained mixture was in turn washed with deionized water 3 times and with ethanol 3 times for the removal of most of the surfactant. After filtration and drying at 80° C overnight, the substance obtained was the $Ca(OH)_2$ intermediate. After thorough grinding, the powders were heated in an oxygen flow of 80 mL/min at a ramp of 1° C/min from room temperature (RT) to 600° C and maintained at this temperature for 3 h. The final product obtained was the single-crystalline wormhole-like mesoporous CaO, denoted as *meso*-CaO.

The *meso*-CaO-supported vanadia catalyst was prepared by means of the incipient wetness impregnation method [8]. In a typical preparation, 2.0 g of the *meso*-CaO support was added to a mixed solution of NH_4VO_3 (0.286 g), oxalic acid (0.440 g), and ethanol (2 mL) under magnetic stirring for 4 h. After being dried at 110° C overnight, the powders were calcined in air (50 mL/min) at a ramp of 1° C/min from RT to 550° C and kept at this temperature for 3 h, thus obtaining 10 wt.% VO_x/*meso*-CaO (denoted as 10V/*meso*-CaO). Following the above procedure and with 10V/*meso*-CaO as support and chromium nitrate as Cr source, we prepared *y*Cr/10V/*meso*-CaO (*y* = 1, 2, and 4 wt.%) catalysts. The VO_x or CrO_x weight percentage referred to the mass content of V_2O_5 or Cr_2O_3 in the catalysts.

2.2. Catalyst characterization

X-ray diffraction (XRD) patterns of *y*Cr/10V/*meso*-CaO (*y* = 0, 1, 2, and 4 wt.%) were recorded on a Bruker/AXS D8 Advance diffractometer using Cu Kα irradiation and nickel filter (λ = 0.15406 nm). The BET surface areas, N_2 adsorption–desorption isotherms, and pore size distributions of the samples were measured by means of a Micromeritics ASAP 2020 instrument. Before the adsorption of N_2 at −196° C, the samples were degassed at 250° C for 3 h. The morphologies of the catalysts were examined using a scanning electron microscope (SEM, Gemini Zeiss Supra 55) operated at 10 kV. Transmission electron microscopic (TEM) images as well as the selected-area electron diffraction (SAED) patterns of the typical samples were obtained using a JEOL JEM-2010 apparatus operated at 200 kV. Raman spectra of the catalysts were collected on a laser Raman equipment (Bruker RFS/100) with a Nd:YAG laser (1064 nm) and an InGaAs detector. The laser power was 100 mW. The sample (0.2 g) was mounted on the stainless steel sample holder in the Raman cell, and the Raman spectra in the shift range of 300–1200 cm^{-1} were collected with a resolution of 4 cm^{-1}. H_2 temperature-programmed reduction (H_2-TPR) experiments were conducted on a Micromeritics AutoChem II 2920 instrument. 50 mg of the sample was placed in a U-shaped quartz tube and treated in oxygen (40 mL/min) at 500° C for 1 h and then cooled down to RT before being reduced in a 5% H_2–95% Ar flow of 30 mL/min at a ramp rate of 10° C/min from RT to 800° C. The thermal conductivity detector (TCD) responses were calibrated against that of the complete reduction of a standard CuO powdered sample (Aldrich, 99.995%).

2.3. Catalytic evaluation

The ODH of isobutane (i.e., *i*-butane or *i*-C_4H_{10}) was carried out in a quartz fixed-bed micro-reactor at atmospheric pressure. Unless specified otherwise, 0.1 g of the catalyst (40–60 mesh) was used and diluted with an equal amount of acid-washed quartz sand (40–60 mesh) in order to minimize the temperature gradient for each test. The flow rate of feed gas mixture (*i*-C_4H_{10}/O_2/N_2 molar ratio = 2:4:44) was 50 mL/min, thus giving a space velocity (SV) of 30,000 mL/(g h). A thermocouple was placed in the middle of the catalyst bed to measure the reaction temperature. The effluent was analyzed on-line using a Shimadzu GC-2010 gas chromatograph equipped with FID and TCD detectors. The aluminum oxide porous layer open tubular (Rt-Alumina PLOT, Restek, USA) capillary column (30 m in length) for FID detector was used to separate the hydrocarbons, whereas the Uni Beads-1S column (3 m in length) for TCD detector was used to separate CO, CO_2, and O_2. The isobutane conversion and product selectivities were calculated based on the balance of carbon.

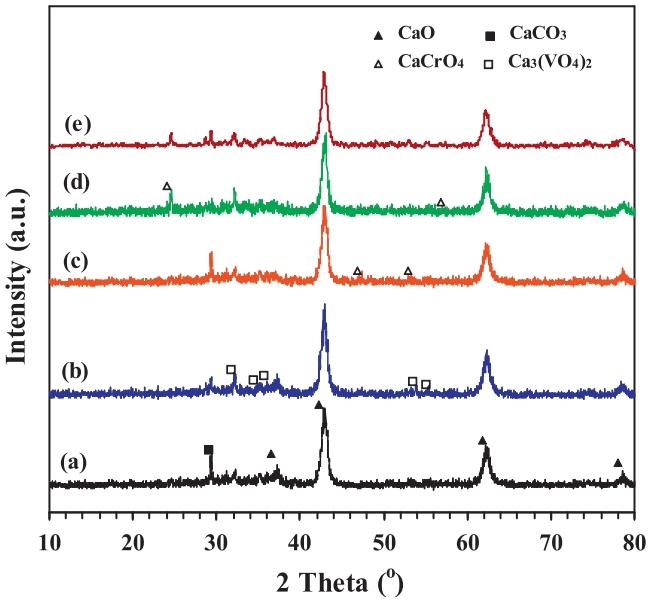

Fig. 1. XRD patterns of (a) *meso*-CaO, (b) 10V/*meso*-CaO, (c) 1Cr/10V/*meso*-CaO, (d) 2Cr/10V/*meso*-CaO, and (e) 4Cr/10V/*meso*-CaO.

3. Results and discussion

The XRD patterns of the as-prepared samples were shown in Fig. 1. It is observed that in addition to the presence of a small amount of the $CaCO_3$ phase (JCPDS PDF# 83-1762), there was the formation of the cubic CaO phase (JCPDS PDF# 82-1690). Loading vanadia and/or chromia on the CaO support resulted in the generation of a small amounts of the orthorhombic $Ca_3(VO_4)_2$ phase (JCPDS PDF# 71-0790) and/or the tetragonal $CaCrO_4$ phase (JCPDS PDF# 75-0936), as indicated in Fig. 1(b–d). The $CaCO_3$ impurity was formed due to the interaction of CaO generated from $Ca(OH)_2$ decomposition and CO_2 emitted from the oxidation of the residual PEG molecules during the calcination process. It should be noted that no Cr_2O_3, V_2O_5, and $CrVO_4$ phases in the Cr–V binary oxide catalysts were detected, as confirmed by the results of Raman studies.

Shown in Fig. 2 are the N_2 adsorption–desorption isotherms and pore size distributions of the *meso*-CaO and *y*Cr/10V/*meso*-CaO samples. It can be observed from Fig. 2A(a) that the CaO support exhibited type IV isotherms, with a big H1 hysteresis loop and a small H3 hysteresis loop in the p/p_0 range of 0.5–0.9 and 0.9–1.0, respectively. Similar dual hysteresis loops have also been observed in the mesoporous CaO and MgO materials [12,13]. The absence of an adsorption isotherm plateau at relative pressure near unity suggests the presence of a small amount of slit-shaped macropores [14], which originated from the aggregates of plate-like particles. The appearance of the big hysteresis loop in the p/p_0 range of 0.5–0.9 indicates the presence of a number of mesopores [15], which originated from the textural pores of the plate-like entities.

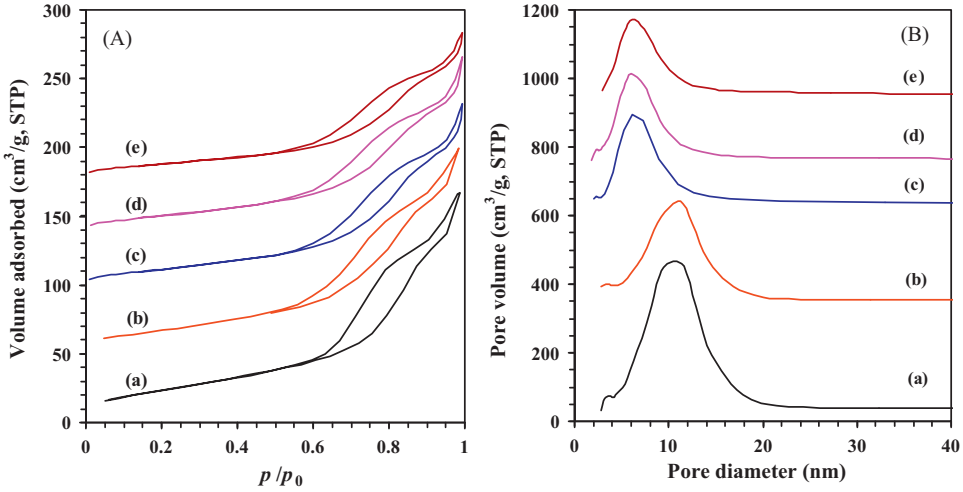

Fig. 2. (A) N_2 adsorption–desorption isotherms and (B) pore size distributions of (a) *meso*-CaO, (b) 10V/*meso*-CaO, (c) 1Cr/10V/*meso*-CaO, (d) 2Cr/10V/*meso*-CaO, and (e) 4Cr/10V/*meso*-CaO.

In other words, there was the co-presence of mesopores (in majority) and macropores (in minority) in the CaO support. The loading of M (M = V or (Cr + V)) did not alter the shape of the N_2 sorption isotherm significantly, indicating that the pore structures of the *y*Cr/10V/*meso*-CaO samples were similar to those of the *meso*-CaO support. From Fig. 2B, one can also see that the mesopore sizes were mainly 6–7 nm for the *y*Cr/10V/*meso*-CaO (*y* = 1, 2, and 4 wt.%) catalysts but 10–11 nm for the CaO and 10V/*meso*-CaO samples. The M surface densities and textural parameters of the *meso*-CaO and *y*Cr/10V/*meso*-CaO samples are summarized in Table 1. The surface areas of *meso*-CaO and *y*Cr/10V/*meso*-CaO (*y* = 0, 1, 2, and 4 wt.%) were 79, 87, 77, 73, and 65 m^2/g, respectively; the corresponding V surface density was 0, 7.6, 8.6, 9.1, and 10.2 V/nm^2, whereas the corresponding Cr surface density was 0, 0, 1.0, 2.2, and 4.9 Cr/nm^2. All of the samples possessed a pore size of 8.9–10.9 nm and a pore volume of 0.18–0.25 cm^3/g.

Representative SEM and TEM images as well as SAED patterns of the *meso*-CaO and *y*Cr/10V/*meso*-CaO samples were shown in Fig. 3. Obviously, the *meso*-CaO and *y*Cr/10V/*meso*-CaO particles displayed similar shapes and sizes. That is to say, loading VO_x and/or CrO_x did not cause considerable changes in morphology and size of the mesoporous CaO support. The samples were mainly composed of tetragonal particles (200–750 nm in length and 50–360 nm in width) and hexagonal particles (60–200 nm in thickness and 80–400 nm in lateral length). From the TEM images of the *meso*-CaO and *y*Cr/10V/*meso*-CaO samples, one can observe the co-presence of tetra- and hexagonal particles with three-dimensional wormhole-like mesopores. The appearance of linear alignments of bright electron diffraction spots in the SAED patterns reveals that the mesoporous CaO support was single-crystalline.

In the past years, Laser Raman spectroscopic technique has been considered as an effective tool to characterize the surface structures of active phases in supported materials. On the surfaces of supported chromia samples, there are three kinds of chromium species: isolated monochromate, polychromate, and crystalline α-Cr_2O_3. It has been reported that the Raman bands at 220, 350, 495, and 986 cm^{-1}, the ones in the 750–1010 cm^{-1} range, and the ones at 550–560 cm^{-1} can be ascribed to the monochromate species of Cr^{6+} state (CrO_3), Cr^{6+} species in the form of polychromate with different degrees of oligomerization, and crystalline α-Cr_2O_3 [3,9,10,16], respectively. Over the supported vanadia samples, the band at 1033 cm^{-1} is assigned to the V=O stretching mode in monovanadate and polyvanadate, and the ones in the range of 750–1000 cm^{-1} are assigned to V–O–V stretching modes in two-dimensional polyvanadate [3,5,17,18]. Crystalline V_2O_5 usually exhibits sharp intense Raman bands at 1002, 708, 535, 490, 410, 305, 289, 203, and 150 cm^{-1} [18–20]. Fig. 4 shows the Raman spectra of the *meso*-CaO-supported catalysts. For the 10V/*meso*-CaO sample, Raman bands appeared at 750, 784, 890, 1030, and 1080 cm^{-1}, indicating that the vanadium species were mono-and polyvanadates [3,5,17,18]. Loading a small amount of chromia on 10V/*meso*-CaO resulted in the decrease in intensity of Raman bands due to the chromium and vanadium species or even the disappearance of their Raman signals, which might be an outcome due to the interference of fluorescence. In addition, one can observe no detection of Raman bands attributable to the crystalline α-Cr_2O_3 [3,9,10], V_2O_5 [18–20], and $CrVO_4$ (930 cm^{-1} [3]) phases. These results reveal that the vanadium and/or chromium species were highly dispersed on the *meso*-CaO surfaces.

It is well known that the ODH of alkanes over supported transition-metal oxides proceeds via a redox mechanism, in which the reducibility is a key factor influencing the performance of the catalyst [8–11]. Shown in Fig. 5 are the H_2-TPR profiles of the as-prepared catalysts. Over 10V/*meso*-CaO, highly dispersed VO_x could be reduced at 578° C, much lower than the reduction temperature (>660° C) of crystalline V_2O_5 [21,22]. With the loading of chromia on 10V/*meso*-CaO, there were three reduction bands at 396, 575, and 625° C (shoulder) over 1Cr/10V/*meso*-CaO, three ones at

Table 1
M surface densities and textural parameters of the as-prepared samples.

Catalyst	Surface area (m^2/g)	V surface density (V/nm^2)	Cr surface density (Cr/nm^2)	M surface density (M/nm^2)	Average pore size (nm)	Pore volume (cm^3/g)
meso-CaO	79	–	–	–	10.1	0.25
10V/*meso*-CaO	87	7.6	–	7.6	10.9	0.24
1Cr/10V/*meso*-CaO	77	8.6	1.0	9.6	9.0	0.20
2Cr/10V/*meso*-CaO	73	9.1	2.2	11.3	8.9	0.21
4Cr/10V/*meso*-CaO	65	10.2	4.9	15.1	8.9	0.18

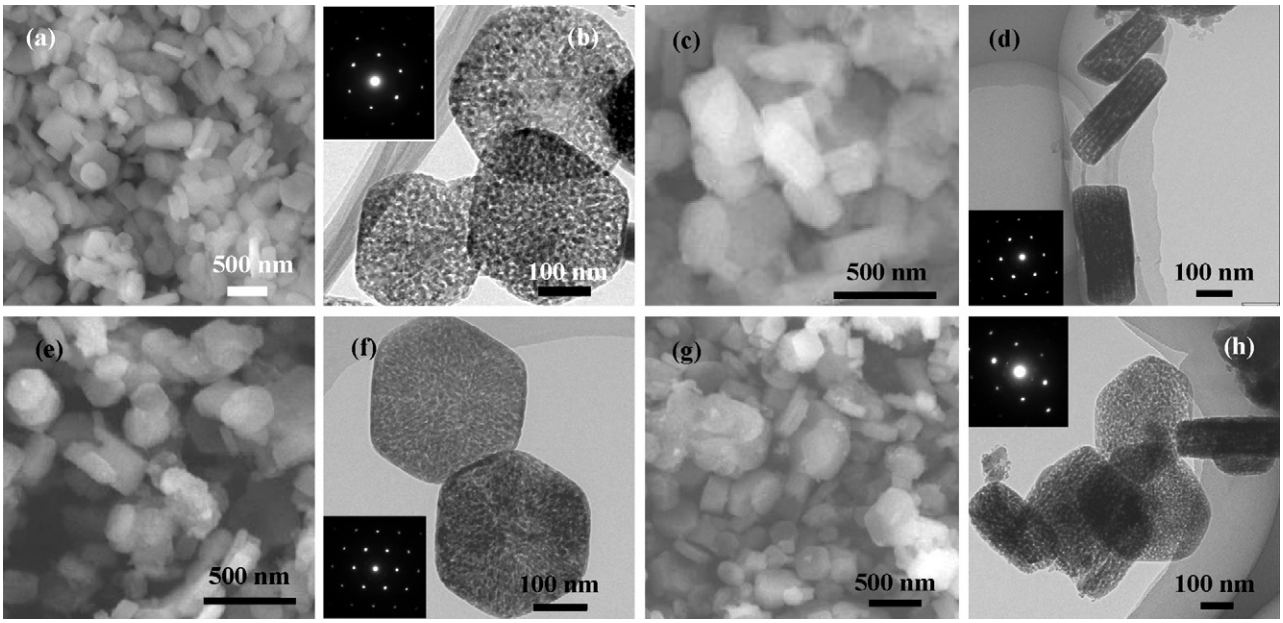

Fig. 3. SEM (a, c, e, and g) and TEM (b, d, f, and h) images as well as the SAED patterns (insets) of (a and b) *meso*-CaO, (c and d) 10V/*meso*-CaO, (e and f) 2Cr/10V/*meso*-CaO and (g and h) 4Cr/10V/*meso*-CaO.

368, 570, and 600° C (shoulder) over 2Cr/10V/*meso*-CaO, and three ones at 388, 480, and 573° C over 4Cr/10V/*meso*-CaO. The loading of chromia on 10V/*meso*-CaO generated more reducible CrO_x species [5], resulting in a decrease in onset reduction temperature (i.e., an enhancement in reducibility). Based on the previous results reported by other researchers [2–5,9–11,21,22], one can reasonably assign the bands below 500° C to the reduction of the tetrahedrally coordinated Cr^{6+} species, whereas those above 500° C to the reduction of VO_x species. The H_2 consumptions were 1.47, 1.66, 1.90, and 2.07 mmol/g_{cat} for the *y*Cr/10V/*meso*-CaO catalysts with *y* = 0, 1, 2, and 4 wt.%, respectively. It is understandable because the reducible chromia amount in the catalyst increased. Usually, it is convenient to compare the reducibility of samples in terms of the initial H_2 consumption rate per mole of metal M (M = V or (Cr + V)) where reduction is less than 20% (i.e., no occurrence of phase transformation). Fig. 5(B) shows the initial H_2 consumption rates of the samples versus inverse temperature. The initial H_2 consumption rate decreased in the order of 2Cr/10V/*meso*-CaO > 4Cr/10V/*meso*-CaO > 1Cr/10V/*meso*-CaO > 10V/*meso*-CaO. The irregular trend of the catalysts in initial H_2 consumption rate can be understandable because formation of more amounts of less reducible $CaCrO_4$ and $Ca_3(VO_4)_2$ (Fig. 1) at a chromia loading of above 2 wt.% was unfavorable for the enhancement in initial H_2 consumption rate.

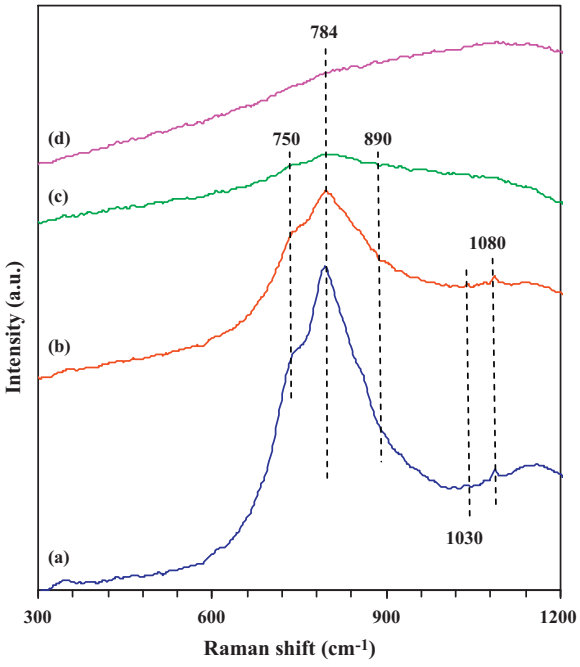

Fig. 4. Laser Raman spectra of (a) 10V/*meso*-CaO, (b) 1Cr/10V/*meso*-CaO, (c) 2Cr/10V/*meso*-CaO, and (d) 4Cr/10V/*meso*-CaO.

Over the *y*Cr/10V/*meso*-CaO catalysts under the conditions of *i*-C_4H_{10}/O_2 molar ratio = 1:2, and SV = 30,000 mL/(g h), isobutane was oxidized to C_4-olefins (i.e., isobutene (main product) + *trans*/*cis*-butenes + butadiene), C_1–C_3 hydrocarbons (i.e., propane + propene + ethane + ethane + methane), and carbon oxides (CO + CO_2) as well as C_4-oxygenates (trace amount). Isobutene accounted for about 95% of C_4-olefins while propene accounted for about 87% of C_1–C_3 hydrocarbons. With a rise in reaction temperature, the isobutane conversion (Fig. 6(A)), C_1–C_3 selectivity (not shown here), and C_4-olefins yield (Fig. 6(C)) increased whereas the C_4-olefins selectivity (Fig. 6(B)) decreased. The highest C_4-olefins yield of 15% at 540° C was achieved over the 2Cr/10V/*meso*-CaO catalyst, with the corresponding isobutane conversion and C_4-olefins selectivity being 19 and 79%. Shown in Fig. 7 are the initial isobutane consumption rate and initial isobutene formation rate as a function of M (M = V or (Cr + V)) surface density at different reaction temperatures. Clearly, both the initial isobutane consumption rate and the isobutene formation rate first increased and then decreased, with the highest values being achieved over the 2Cr/10V/*meso*-CaO catalyst (M surface density = 11.3 M/nm^2); the initial isobutane consumption rate and isobutene formation rate increased with increasing the reaction temperature.

For comparison purpose, we also prepared the 2Cr/*meso*-CaO (Cr surface density = 3.2 Cr/nm^2) and 2Cr/10V/*bulk*-CaO (M surface density = 88.2 M/nm^2) catalysts and evaluated their catalytic activities under the same reaction conditions. It is found that the catalytic performance of 2Cr/*meso*-CaO (C_4-olefins selectivity = 63.8%, C_4-olefins yield = 8.2% at 540° C) and 2Cr/10V/*bulk*-CaO (C_4-olefins

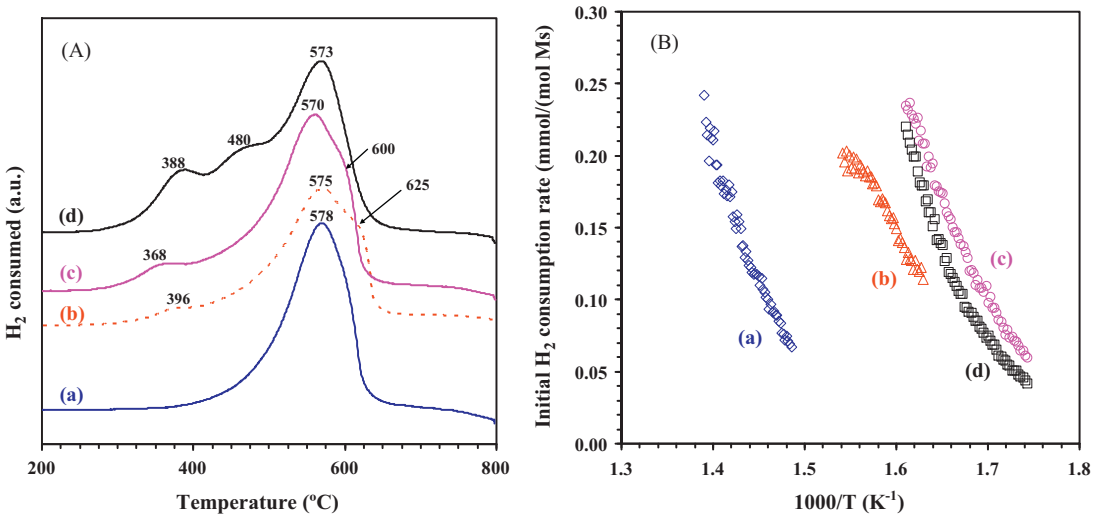

Fig. 5. (A) H_2-TPR profiles and (B) initial H_2 consumption rate of (a) 10V/*meso*-CaO, (b) 1Cr/10V/*meso*-CaO, (c) 2Cr/10V/*meso*-CaO, and (d) 4Cr/10V/*meso*-CaO.

selectivity = 20.0%, C_4-olefins yield = 3.0% at 540° C) were much inferior to that of 2Cr/10V/*meso*-CaO (C_4-olefins selectivity = 79%, C_4-olefins yield = 15% at 540° C) and that of 10V/*meso*-CaO (C_4-olefins selectivity = 71.6%, C_4-olefins yield = 10.8% at 540° C). The presence of three-dimensional wormhole-like mesoporous structure (Figs. 2 and 3) might facilitate the dispersion of a higher amount of isolated and low polymeric chromium and vanadium species (Fig. 4) on the surface of *meso*-CaO [2], and the diffusion of reactant molecules (thus minimizing the deep oxidation of the C_4-olefins products [10]). Thus, 2Cr/10V/*meso*-CaO gave better catalytic performance than 2Cr/10V/*bulk*-CaO.

Due to the high electron densities at the π band, alkenes are generally considered to be basic [23]. A more basic surface would prefer a faster desorption of olefins before their deep oxidation to CO_x [11]. It has been generally accepted that olefins selectivity goes up with a decrease in acidity and an increase in basicity of the catalyst [24–26]. Since the basicity of $CaCO_3$ is lower than that of CaO, the formation of $CaCO_3$ (Fig. 1) would lead to a drop in C_4-olefins selectivity of the *y*Cr/10V/*meso*-CaO catalysts. Under the same reaction conditions, the catalytic activity of 2Cr/10V/*meso*-CaO (C_4-olefins yield = 15%) was better than that of 8 wt.% $CrO_x/Ce_{0.60}Zr_{0.35}Y_{0.05}O_2$ (C_4-olefins yield = 10%) [9], 10 wt.% CrO_x/SBA-15 (C_4-olefins yield = 11%) [10], and Cr–Mo binary oxide supported on MgO-coated SBA-16 (C_4-olefins yield = 7.5%) [11] previously reported by our group. Furthermore, such a performance obtained over the 2Cr/10V/*meso*-CaO catalyst (C_4-olefins yield = 15% at 540° C) was much superior to those achieved over K–CrO_x/SiO_2 (C_4-olefin yield = 5.8% at 525° C) [27], 10 wt.% CrO_x/Al_2O_3 (C_4-olefin yield = 6.0% at 250° C) [28], and [Si, V]-MCM-41 (C_4-olefin yield = 5.2% at 550° C) [29]. In addition to the acidity/basicity and pore structure of the support employed, the discrepancy in catalytic performance of these catalysts is also associated with the active phase (CrO_x or VO_x) dispersion and reducibility. According to the results of the XRD and Raman characterization (Figs. 1 and 4), most of VO_x and/or CrO_x were highly dispersed in the form of mono- and polyvanadate or polychromate on the surface of the *meso*-CaO support. The loading of more reducible CrO_x on 10V/*meso*-CaO might cause a decrease in the V–O–Ca linkage and an increase in the V–O–Cr linkage of the *y*Cr/10V/*meso*-CaO catalysts, thus enhancing the reducibility (Fig. 5). Similar loading effects have also been reported in the $V/Mo/Al_2O_3$ [8] and $Cr/V/Al_2O_3$ catalysts [20]. The co-presence of multiple coordinated vanadate or chromate in the *y*Cr/10V/*meso*-CaO catalysts was beneficial for the facile redox action in which lattice oxygen involved in the ODH of isobutane [10]. The reactivity of lattice oxygen was related to the initial H_2 consumption rate of the catalyst. As revealed in the H_2-TPR studies (Fig. 5), the initial H_2 consumption rate followed the sequence of 2Cr/10V/*meso*-CaO > 4Cr/10V/*meso*-CaO > 1Cr/10V/*meso*-CaO > 10V/*meso*-CaO, in rough agreement with the C_4-olefins selectivity order (4Cr/10V/*meso*-CaO > 2Cr/10V/*meso*-CaO > 1Cr/10V/*meso*-CaO > 10V/*meso*-CaO). Although 4Cr/10V/*meso*-CaO showed a higher C_4-olefins selectivity than 2Cr/10V/*meso*-CaO, the isobutane conversion over the former

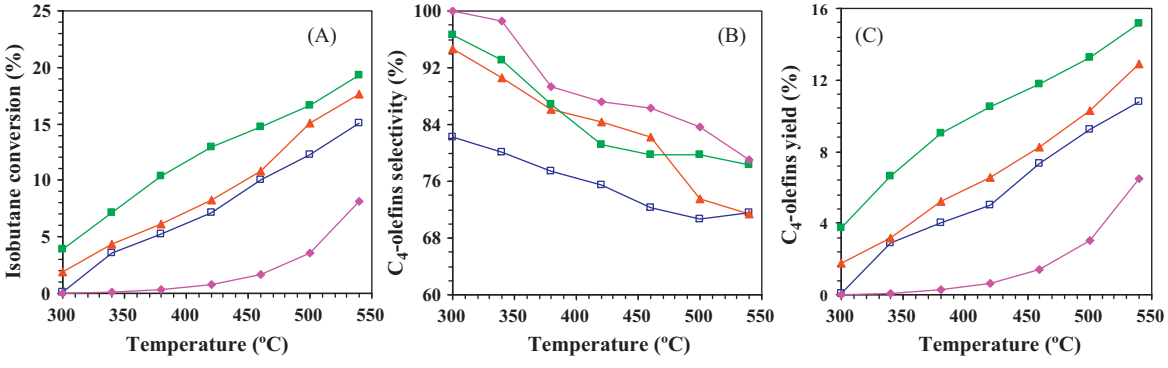

Fig. 6. (A) i-C_4H_{10} conversion, (B) C_4-olefins selectivity, and (C) C_4-olefins yield as a function of reaction temperature obtained over (□) 10V/*meso*-CaO, (▲) 1Cr/10V/*meso*-CaO, (■) 2Cr/10V/*meso*-CaO, and (◆) 4Cr/10V/*meso*-CaO.

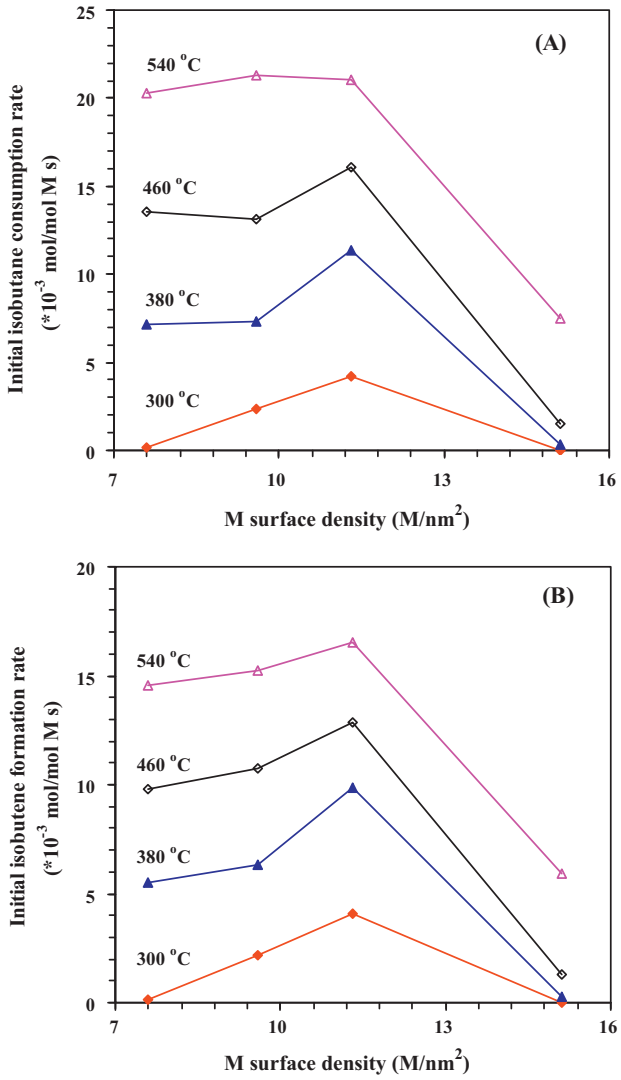

Fig. 7. Effects of M surface density on (A) isobutane consumption rate and (B) isobutene formation rate over the *y*Cr/10V/*meso*-CaO (*y* = 0, 1, 2, and 4 wt.%) catalysts.

was much lower than that over the latter, thus resulting in a significant drop in C_4-olefins yield over 4Cr/10V/*meso*-CaO (Fig. 6). Such an outcome might be due to the generation of more amounts of less active $CaCrO_4$ and $Ca_3(VO_4)_2$ (Fig. 1).

4. Conclusions

By adopting the incipient wetness impregnation method, bulk CaO and single-crystalline wormhole-like mesoporous CaO supported catalysts (2Cr/*meso*-CaO, *y*Cr/10V/*meso*-CaO (*y* = 0, 1, 2, and 4 wt.%), and 2Cr/10V/*bulk*-CaO) were prepared. The XRD results reveal that there was formation of small amounts of $CaCO_3$, $Ca_3(VO_4)_2$, and $CaCrO_4$ phases in the vanadia- and/or chromia-loaded *meso*-CaO catalysts. The BET and TEM results indicate that the wormhole-like mesoporous structures were retained in *y*Cr/10V/*meso*-CaO. The results of Raman investigations suggest that VO_x and/or CrO_x were highly dispersed in the form of mono- and polyvanadate and/or polychromate on the surface of the *meso*-CaO support. Loading more reducible chromia could improve the reducibility of 10V/*meso*-CaO, and the 2Cr/10V/*meso*-CaO catalyst possessed the best low-temperature reducibility among the as-prepared catalysts. Under the conditions of isobutane/O_2 molar ratio = 1/2, space velocity = 30,000 mL/(g h), and temperature = 540° C, the 2Cr/10V/*meso*-CaO catalyst performed the best, giving a C_4-olefins yield of 15% with the corresponding C_4-olefins selectivity of 79%. It is concluded that the excellent catalytic performance of 2Cr/10V/*meso*-CaO was associated with the high dispersion of CrO_x and VO_x domains and good low-temperature reducibility as well as the strong basicity and three-dimensional wormhole-like mesoporosity of the CaO support.

Acknowledgements

This work was supported by the NSF of China (Grant Nos. 20973017 and 20473006), and the PHR200907105 of the Beijing Municipal Commission of Education.

References

[1] F. Cavani, N. Ballarini, A. Cericola, Catal. Today 127 (2007) 113–131.
[2] Y.-M. Liu, Y. Cao, N. Yi, W.-L. Feng, W.-L. Dai, S.-R. Yan, H.-Y. He, K.-N. Fan, J. Catal. 224 (2004) 417–428.
[3] S.W. Yang, E. Iglesia, A.T. Bell, J. Phys. Chem. B 110 (2006) 2732–2739.
[4] S.A. Karakoulia, K.S. Triantafyllidis, G. Tsilomelekis, S. Boghosian, A.A. Lemonidou, Catal. Today 141 (2009) 245–253.
[5] B. Mitra, I.E. Wachs, G. Deo, J. Catal. 240 (2006) 151–159.
[6] A. Klisińska, K. Samson, I. Gressel, B. Grzybowska, Appl. Catal. A 309 (2006) 10–16.
[7] K.D. Chen, S.B. Xie, E. Iglesia, A.T. Bell, J. Catal. 189 (2000) 421–430.
[8] H.X. Dai, A.T. Bell, E. Iglesia, J. Catal. 221 (2004) 491–499.
[9] G.Z. Wang, H.X. Dai, L. Zhang, J.G. Deng, C.X. Liu, H. He, C.T. Au, Appl. Catal. A 375 (2010) 272–278.
[10] G.Z. Wang, L. Zhang, J.G. Deng, H.X. Dai, H. He, C.T. Au, Appl. Catal. A 355 (2009) 192–201.
[11] L. Zhang, J.G. Deng, H.X. Dai, C.T. Au, Appl. Catal. A 354 (2009) 72–81.
[12] C.X. Liu, L. Zhang, J.G. Deng, Q. Mu, H.X. Dai, H. He, J. Phys. Chem. C 112 (2008) 19248–19256.
[13] G.Z. Wang, L. Zhang, H.X. Dai, J.G. Deng, C.X. Liu, H. He, C.T. Au, Inorg. Chem. 47 (2008) 4015–4022.
[14] W.C. Li, A.H. Lu, C. Weidenthaler, F. Schüth, Chem. Mater. 16 (2004) 5676–5681.
[15] L. Gou, C.J. Murphy, J. Mater. Chem. 14 (2004) 735–738.
[16] B. Grzybowska, J. Sloczyński, R. Grabowski, K. Wcislo, A. Kozlowska, J. Stoch, J. Zieliński, J. Catal. 178 (1998) 687–700.
[17] I. Rossetti, L. Fabbrini, N. Ballarini, C. Oliva, F. Cavani, A. Cericola, B. Bonelli, M. Piumetti, E. Garrone, H. Dyrbeck, E.A. Blekkan, L. Forni, J. Catal. 256 (2008) 45–61.
[18] B. Kilos, A.T. Bell, E. Iglesia, J. Phys. Chem. C 113 (2009) 2830–2836.
[19] G. Du, S. Lim, M. Pinault, C. Wang, F. Fang, L. Pfefferle, G.L. Haller, J. Catal. 253 (2008) 74–90.
[20] S.W. Yang, E. Iglesia, A.T. Bell, J. Phys. Chem. B 109 (2005) 8987–9000.
[21] O. Schwarz, D. Habel, O. Ovsitser, E.V. Kondratenko, C. Hess, R. Schomäcker, H. Schubert, J. Mol. Catal. A 293 (2008) 45–52.
[22] W. Liu, S.Y. Lai, H.X. Dai, S.J. Wang, H.Z. Sun, C.T. Au, Catal. Lett. 113 (2007) 147–154.
[23] R.X. Valenzuela, V. Cortés Corberán, Top. Catal. 11–12 (2000) 153–160.
[24] A. Klisińska, S. Loridant, B. Grzybowska, J. Stoch, I. Gressel, Appl. Catal. A 309 (2006) 17–27.
[25] W. Liu, S.Y. Lai, H.X. Dai, S.J. Wang, H.Z. Sun, C.T. Au, Catal. Today 131 (2008) 450–456.
[26] G. Neri, A. Pistone, S. De Rossi, E. Rombi, C. Milone, S. Galvagno, Appl. Catal. A 260 (2004) 75–86.
[27] R. Grabowski, B. Grzybowska, J. Słoczyńki, K. Wcisło, Appl. Catal. A 144 (1996) 335–341.
[28] B. Grzybowska, J. Słoczyńki, R. Grabowski, K. Wcisło, A. Kozłowska, J. Stoch, J. Zieliński, J. Catal. 178 (1998) 687–700.
[29] B. Sulikowski, Z. Olejniczak, E. Wloch, J. Rakoczy, R.X. Valenzuela, V.C. Corberán, Appl. Catal. A 232 (2002) 189–202.